Polymeric Multilayer Capsule-Mediated Vaccination Induces Protective Immunity Against Cancer and Viral Infection

Bruno G. De Geest,[†,*] Monique A. Willart,[‡,§] Hamida Hammad,[‡,§] Bart N. Lambrecht,[‡,§] Charlotte Pollard,[#,⊥] Pieter Bogaert,[§] Marina De Filette,[§,⊥] Xavier Saelens,[§,⊥] Chris Vervaet,[†] Jean Paul Remon,[†] Johan Grooten,[⊥,∥] and Stefaan De Koker[⊥,∥]

[†]Laboratory of Pharmaceutical Technology, Department of Pharmaceutics and [‡]Laboratory of Immunoregulation and Mucosal Immunology, Department of Pulmonary Medicine, Ghent University, Ghent, Belgium, [§]Department of Molecular Biomedical Research, VIB, Zwijnaarde, Belgium, [⊥]Department of Biomedical Molecular Biology, Ghent University, Zwijnaarde, Belgium, and [#]Institute of Tropical Medicine of Antwerp, Department of Microbiology, Unit Virology, Antwerp, Belgium. [∥]These authors equally supervised this work.

ABSTRACT Recombinant antigens hold high potential to develop vaccines against lethal intracellular pathogens and cancer. However, they are poorly immunogenic and fail to induce potent cellular immunity. In this paper, we demonstrate that polymeric multilayer capsules (PMLC) strongly increase antigen delivery toward professional antigen-presenting cells *in vivo*, including dendritic cells (DCs), macrophages, and B cells, thereby enforcing antigen presentation and stimulating T cell proliferation. A thorough analysis of the T cell response demonstrated their capacity to induce IFN-γ secreting CD4 and CD8 T cells, in addition to follicular T-helper cells, a recently identified CD4 T cell subset supporting antibody responses. On the B cell level, PMLC-mediated antigen delivery promoted the formation of germinal centers, resulting in increased numbers of antibody-secreting plasma cells and elevated antibody titers. The functional relevance of the induced immune responses was validated in murine models of influenza and melanoma. On a mechanistic level, we have demonstrated the capacity of PMLC to activate the NALP3 inflammasome and trigger the release of the potent pro-inflammatory cytokine IL-1β. Finally, using DC-depleted mice, we have identified DCs as the key mediators of the immunogenic properties of PMLC.

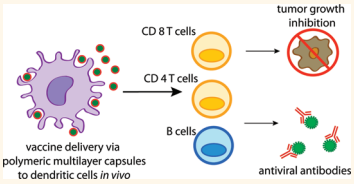

KEYWORDS: capsules · vaccines · self-assembly · polyelectrolytes · layer-by-layer · dendritic cells

Many of the most effective vaccines we have today are based on the parenteral delivery of attenuated variants of pathogens. These living vectors efficiently deliver the relevant antigens to the immune system and also activate the innate immune system to evoke robust and sometimes life-long lasting antibody and T cell immune responses.[1] Nevertheless, as these vaccines are composed of living vectors, they might impose serious safety issues. In addition, in those cases where natural infection does not generate adequate immunity, for example, because immune responses are directed against hypervariable antigen domains, the use of attenuated vaccines has been unsuccessful.[2] Driven by these issues, focus on vaccine design has shifted from whole microorganism vaccines toward the development of entirely synthetic vaccines composed of recombinant antigens.[2,3] Most of these recombinant antigens are, however, poorly immunogenic and thus require the addition of adjuvants to elicit protective immunity. Unfortunately, for insidious pathogens such as HIV, malaria, and tuberculosis, the currently licensed adjuvants for human use, the aluminum salts (alum) and the oil-in-water emulsion MF59, fail to induce potent CD4 Th1 and CD8 cytotoxic T cell responses, which are required to prevent or control infection.[4,5] In addition, CD8 T cells also have the capacity to kill tumor cells, making therapeutic cancer vaccination an interesting option to control or even eliminate metastases.[6,7] Moreover, although aluminum salts as well as MF59 are fairly potent inducers of antibody responses against co-delivered antigens,[8−10] for some pathogens and patient groups, seroconversion or protective antibody titers are not reached using these adjuvants. As a consequence, the need for more potent adjuvants stimulating strong and long lasting B cell responses remains to date.[11] Thereby, designing novel adjuvants that simultaneously generate potent humoral and cellular immune responses still represents a major challenge.

* Address correspondence to br.degeest@ugent.be.

Received for review October 17, 2011 and accepted February 3, 2012.

Published online February 03, 2012
10.1021/nn205099c

Formulating protein antigens in nano/microparticulate carriers has emerged as one of the most promising strategies to modulate and increase immune response to vaccine antigens.[12−16] Particles in in the 0.1−10 μm range resemble the dimensions of viruses and bacteria and are far better recognized and processed by professional antigen-presenting cells (APCs) when compared to soluble antigens. The most potent APCs are the dendritic cells (DCs), innate immune cells specialized at engulfing micro-organisms and presenting their antigens to T cells in the draining lymph nodes. Formulating antigen in nano- or microparticles leads to increased antigen uptake by DCs. This increases the strength of the elicited T cell response but also affects its quality. Indeed, while soluble antigens are almost exclusively presented to CD4 T cells following endocytosis by DCs, antigens in a particulate form can be presented *via* MHCI and MHCII. This allows the simultaneous induction of both CD4 as well as CD8 T cell responses that are crucial to eliminate infected as well as malignant cells. Besides priming T cell responses, DCs also strongly affect the magnitude and quality of the B cell response, by transporting the antigen to B cells in the residing B cell follicles, as well as by stimulating CD4 follicular T helper responses.[17]

Recently, polymeric multilayer capsules (PMLC)[18−21] have been explored as antigen carriers.[22−25] PMLCs are assembled under all aqueous conditions without using reactive chemicals, organic solvents, or high energy input which could potentially lead to antigen denaturation and residual traces of toxic organic compounds that would impair further clinical development. PMLCs are fabricated in three major steps. In a first step, antigen is encapsulated in sacrificial porous[26,27] microtemplates. In a second step, these microtemplates are coated in a layer-by-layer (LbL)[28] fashion with polymers, using electrostatic interactions or hydrogen bonding as the driving force for multilayer build up. Third, the sacrificial microtemplates are decomposed into low molecular weight components. As the polyelectrolyte shell is semipermeable, the dissolved low molecular weight components can freely diffuse outward while (high molecular weight) antigen remains entrapped within the resulting hollow capsules. This hollow nature makes PMLCs closely resemble the morphologic nature of bacteria. While the capsules' shell remains stable under physiological conditions, it rapidly ruptures upon cellular uptake when using biodegradable polyelectrolytes, allowing a fast intracellular release and processing of encapsulated antigen.[29]

Previously, we have shown that PMLC based on dextran sulfate (DS) and poly-L-arginine (P_LARG) are biodegradable *in vitro*[30] and *in vivo*.[31] Subcutaneous injection induces a mild inflammatory reaction restricted to the injection site, similar to FDA approved aluminum salts. Capsules composed of one bilayer were prone to fast mechanical deformation and rupture, while capsules composed of two or more bilayers were more resilient and thus more likely to retain their antigen payload prior to internalization by phagocytic cells. Furthermore, we have demonstrated that antigen encapsulated in PMLC composed of two DS/P_LARG bilayers is readily processed by DCs *in vitro*, resulting in an increased antigen presentation to CD4 and CD8 T cells.[23] In a subsequent study, DS/P_LARG capsules were evaluated as antigen carriers for pulmonary vaccination.[25] Intratracheal instillation of PMLC resulted in the efficient uptake by alveolar macrophages and DCs, followed by the initiation of a Th17 skewed immune response, which is considered to compose a crucial part of the mucosal immune defense against fungi and extracellular bacteria. Importantly, when compared to a mixture of soluble antigen and empty capsules, antigen encapsulation inside the PMLC strongly augmented the strength of this local mucosal immune response, clearly demonstrating the necessity of antigen encapsulation for optimal induction of immunity by PMLC.

In this paper, we aim to provide a more detailed picture of the interactions between DS/P_LARG capsules and the immune system following parenteral delivery of these capsules. Thereby, we have evaluated the capacity of PMLC to deliver antigen to professional APCs (DCs, macrophages, and B cells) as well as its repercussions on antigen presentation to T cells *in vivo*. To characterize the ensuing adaptive immune response, an in-depth analysis of T and B cell responses following immunization with ovalbumin-loaded capsules is provided. The functional relevance of these findings is addressed by exploring for the first time the capacity of PMLC-based immunization in providing protective immunity murine models of cancer (B16 melanoma) and infection (influenza). On a mechanistic level, we have identified DCs as the crucial mediators of the adjuvant properties of PMLC. In addition, in agreement with recent findings obtained using other particulate materials such as aluminum salts, silica beads, and PLGA microparticles,[32] we demonstrate that high doses of PMLC activate the NALP inflammasome, an inflammatory signaling complex triggered by various adjuvants.

RESULTS AND DISCUSSION

Synthesis and Characterization of Polyelectrolyte Multilayer Capsules. Antigen-loaded PMLCs were prepared as schematically shown in Figure 1A. Ovalbumin (OVA; used as model antigen) was encapsulated in PMLC through co-precipitation in calcium carbonate ($CaCO_3$).[33] By mixing equimolar amounts of $CaCl_2$ and Na_2CO_3 in the presence of proteins, highly porous $CaCO_3$ microparticles with a mean diameter of 3 μm (as measured by laser diffraction and confirmed by optical

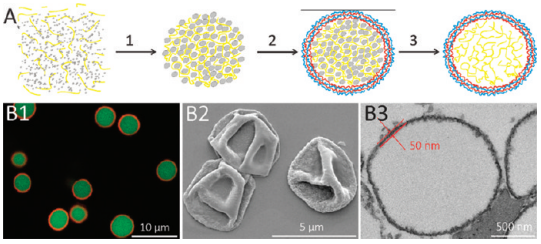

Figure 1. Synthesis and characterization of PMLCs. (A) Schematic representation of the synthesis of hollow antigen-loaded polyelectrolyte multilayer capsules in three steps comprising co-precipitation of antigen (*e.g.*, ovalbumin) and calcium carbonate in a first step, LbL coating of the calcium carbonate microparticles in a second step, and dissolution of the calcium carbonate templates in an aqueous EDTA solution in a third step. (B) Microscopic visualization of PMLCs. (B1) Confocal microscopy image of PMLC using AF488 (green fluorescence)-conjugated ovalbumin and rhodamine (red fluorescence) conjugated poly-L-arginine. (B2) Scanning electron microscopy image of PMLC in a dried state. (B3) Transmission election microscopy image of ultramicrotomed capsules. The arrows in red indicate an approximate shell thickness of 50 nm.

microscopy) were obtained. These particles were subsequently coated in an LbL fashion with two bilayers of dextran sulfate (DS; polyanion, bearing a net negative charge) and poly-L-arginine (P_LARG; polycation, bearing a net positive charge). Zeta-potential values of the microparticles during polyelectrolyte deposition switched from negative to positive, ending with a value of 25 ± 7 mV with poly-L-arginine as outermost layer, in accordance with our previous findings.[34] Following the deposition of the outermost poly-L-arginine layer, the $CaCO_3$ core was removed using EDTA, yielding hollow capsules composed of a nanothin polyelectrolyte multilaylayer membrane. Although the positively charged P_LARG was deposited as the outer layer, dissolution of the $CaCO_3$ core by EDTA switched the zeta-potential back to a negative value of -55 ± 4 mV, a feature attributed to the release of excess DS from the $CaCO_3$ and subsequent rearrangement of the capsules' shell.[34] Figure 1B1 shows a confocal microscopy image of PMLC containing rhodamine isothiocyanate (RITC)-labeled poly-L-arginine to visualize the capsule shell and Alexa Fluor 488 (AF488)-labeled ovalbumin (OVA-AF488) to visualize encapsulated antigen. The collapsed state upon drying, as visualized by scanning electron microscopy (Figure 1B2), demonstrates the deformability of the capsules' membrane, which had a diameter of approximately 50 nm as estimated by transmission electron microscopy taken from capsules that were embedded in an epoxy resin to conserve their spherical shape (Figure 1B3). Taken together, these data demonstrate that LbL coating of antigen-loaded $CaCO_3$ microparticles with DS and P_LARG is well-suited to obtain a stable, nonaggregated capsule suspension.

PMLCs composed of "biopolymers" such as polysaccharides and polypeptides are often reported to have inferior mechanical properties and are more prone to aggregation than their synthetic nondegradable counterparts such as poly(styrene sulfonate) (PSS), poly(allylamine) hydrochloride (PAH), and poly(diallyl dimethyl ammoniumchloride) (PDADMAC).[35] Indeed, we previously reported on LbL coating of hydrogel beads by a series of "biopolyelectrolytes".[35] In that study, we observed that polyelectrolytes that bear a low charge density and high viscosity in aqueous medium, such as hyaluronic acid and chitosan, are extremely prone to capsule aggregation. Furthermore, we found that polyelectrolyte pairs containing a weak (*i.e.*, only charged over a limited pH range) biopolyelectrolyte such as poly-L-glutamic acid or poly-L-aspartic acid are extremely susceptible to capsule rupturing upon dissolution of the hydrogel core templates which exert considerable osmotic pressure on the capsule shell.[36−38] In collaboration with the Auzély group, it was demonstrated that by closely monitoring and optimizing polyelectrolyte assembly conditions nonaggregated hyaluronic acid containing capsules can be fabricated, although these are very brittle and strongly swell in physiological media.[39] However, by using strong biopolyelectrolytes such as dextran sulfate (DS) and poly-L-arginine (P_LARG), which are highly charged over a broad pH range, assembly into stable and nonaggregated capsules can be readily achieved without special precautions during capsule synthesis.[30] Other groups, including the Haynie,[40] Sukhorukov,[41] and Caruso[27] groups, also reported successful fabrication of multilayer capsules composed of biopolyelectrolytes.

When measuring antigen encapsulation efficiency, we were challenged by the high stability of the DS/P_LARG electrostatic complexation. Both of these polymers are strong polyelectrolytes that form stable complexes over the whole pH range. Attempts to decompose these capsules using methods, such as high salt concentrations,[42] acid, or alkaline treatment[43] as well as the use of surfactants,[44] reported for capsules composed of at least one weak polyelectrolyte or template on nonporous microparticles leading to thinner and thus weaker shells, were unsuccessful. Thereby, antigen encapsulation efficiency was solely measurable *via* an indirect method by collecting the supernatants during $CaCO_3$ co-precipitation, LbL coating, and $CaCO_3$ template dissolution and measuring the protein concentration in the respective samples *via* Bradford assay.[23,25] We observed, in agreement with previous reports by the Sukhorukov group, that co-precipitation of proteins with $CaCO_3$ is a highly efficient process leading to no detectable antigen in the supernatant, while we measured full recovery of OVA when dissolving (uncoated) $CaCO_3$ microparticles in aqueous EDTA solution.[45] No significant antigen leakage from these $CaCO_3$ templates was detectable during the LbL coating process. In contrast, upon dissolution of the

$CaCO_3$ cores by EDTA treatment, approximately half of the amount of antigen was released from the capsules, yielding a total antigen encapsulation efficiency of about 50%.[23,25] This efficiency is reasonably high compared to other hollow particulate systems such as liposomes and PLGA particles and slightly lower than a newly reported procedure to formulate antigen in cross-linked multilamellar liposomal vesicles.[14] However, to further maximize the encapsulation efficiency, we are currently developing new strategies to produce polyelectrolyte-based capsules.[46,47]

Analysis of the *In Vitro* Interactions between PMLCs and DCs. As DCs are the main target population of any novel vaccination strategy,[48] we carefully analyzed the interactions between PMLCs and DCs *in vitro*. As depicted in Figure 2A, DCs readily internalize PMLC-encapsulated OVA (Figure 2A1, OVA-labeled green fluorescent with AF488) as is the case for soluble OVA (Figure 2A2, OVA-labeled red fluorescent with AF555). Interestingly, as shown in Figure 2A3, depicting DCs incubated with both soluble OVA-AF555 and encapsulated OVA-AF488, soluble and encapsulated OVA predominantly ends up in different intracellular compartments (the yellow arrow in Figure 2A3 indicates a rare event where green and red fluorescence colocalize). This suggests a different uptake route and intracellular trafficking between soluble and PMLC-encapsulated OVA. Indeed, while soluble OVA is reported to be taken up by receptor-mediated endocytosis or micropinocytosis resulting in its intracellular trafficking to endosomes or lysosomes, PMLCs are taken up by phagocytosis or even macropinocytosis.[23] Consequently, antigen delivery *via* PMLC targets antigen toward phagosomal vesicles, a feature which is likely to affect the magnitude and quality of the elicited T cell response, as phagosomes have been described to be fully competent organelles for antigen presentation, especially augmenting MHCI-mediated antigen presentation toward CD8 T cells.[49]

Earlier, we have demonstrated that DS/P_LARG capsules enhance antigen presentation of encapsulated antigen by DCs *in vitro*.[23] To become fully competent APCs capable of priming naïve T cells, DCs also need to become activated in order to upregulate their expression of co-stimulatory molecules and MHCII. Strong DC activation is typically induced in response to conserved microbial structures such as cell wall components (*e.g.*, LPS, peptidoglycan) and viral nucleic acid structures (uncapped RNA, dsRNA) that trigger pattern recogition receptors (PRRs). Incubation of bone marrow derived DCs with nontoxic amounts of PMLC did not evoke significant DC maturation, as we did not observe a significant upregulation of the DC activation markers CD40 and CD86 by flow cytometry. In contrast, incubation of DCs with the potent TLR4 stimulus LPS readily evoked DC maturation (Figure 2B). Similar observations have been reported by others using a diverse spectrum of microparticles including PLGA,[50] showing that particle phagocytosis by itself not necessary triggers potent DC activation. Nevertheless, recent studies have implicated that part of the adjuvant properties of many particulate structures might be attributed to the activation of an inflammatory signaling platform called the NALP3 inflammasome.[32] Inflammasome activation leads to the activation of caspase-1, which converts the biologically inactive pro-IL-1β to the potent inflammatory cytokine IL-1β. To address the capacity of PMLCs to activate the NALP3 inflammasome, DCs were incubated with a dilution series of PMLC either alone or in combination with low doses of LPS (10 ng/mL). The low doses of LPS is necessary to produce the immature pro-IL-1β, but by itself, it is insufficient to produce the mature IL-1β. Following a 24 h incubation period, the amount of IL-1β released in the culture supernatant was measured by ELISA. As shown in Figure 2C, LPS alone or PMLC alone fails to trigger significant IL-1β release. In contrast, combining low levels of LPS with high amounts of capsules per DC causes a vast secretion of IL-β. To ascertain that this phenomenon was indeed NALP3-dependent, DCs generated from NALP3-deficient knockout mice (NALP3$^{-/-}$) were incubated with the same doses of LPS and capsules. From the dramatic drop in IL-β production observed in NALP3$^{-/-}$ when compared to wild-type mice in response to incubation with high levels of capsules and LPS, it can be concluded that PMLCs indeed are capable of activating the NALP inflammasome.

PMLC-Mediated Antigen Delivery Enhances In Vivo Antigen Uptake and Presentation. The primary goal of this work is to evaluate the potential of PMLCs to enhance antigen delivery toward APCs *in vivo* and to assess the impact of PMLC-mediated antigen delivery on the nature and magnitude of the elicited adaptive immune response. In contrast to soluble antigens and ultrasmall particles in the nanorange (<40 nm), PMLCs are too large to passively drain with the interstitial fluid to the draining lymph nodes. Consequently, APCs need to be recruited to the injection site in order to actively transport the particles to the draining lymph nodes. As demonstrated in Figure 3A, subcutaneous microcapsule injection resulted in a fast influx of cells expressing high levels of MHCII, where expression is limited to professional APCs, surrounding the injection site (Figure 3A2). To address whether PMLCs reach the draining lymph nodes following subcutaneous injection, mice were injected in the footpad with PMLC-encapsulated OVA-AF488, and 48 h later, popliteal lymph nodes were dissected and analyzed by fluorescence microscopy. As shown in Figure 3B,C, a capsule containing cells can be readily observed in the draining lymph nodes following subcutaneous injection, with most of the particles clearly being present in the T cell zone.

To address to what extent antigen encapsulation inside PMLCs augments antigen delivery toward APCs

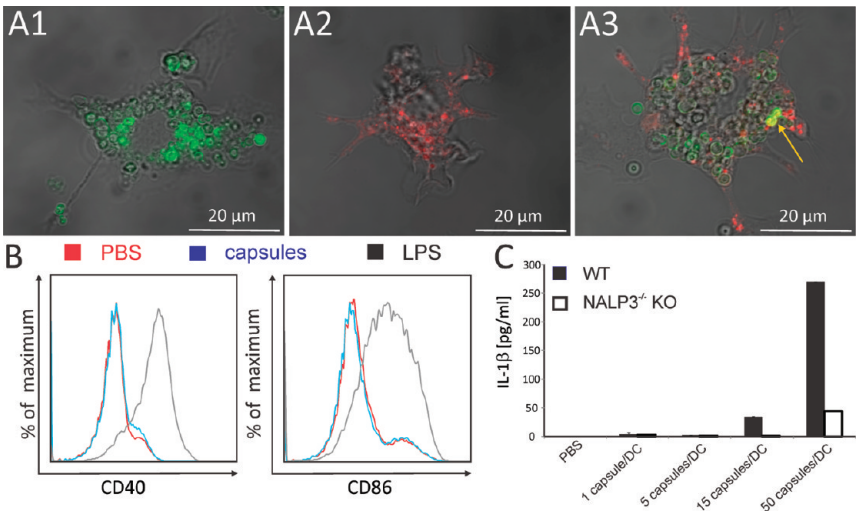

Figure 2. ***In vitro*** **interaction between DCs and PMLCs. (A) Confocal microscopy images of DCs co-incubated with, respectively, (A1) PMLC-encapsulated OVA-AF488 (green fluorescence), (A2) soluble OVA-AF555 (red fluorescence), and (A3) both PMLC-encapsulated OVA-AF488 and soluble OVA-AF555. Each panel shows the overlay of DIC and fluorescence. The yellow arrow in panel C3 indicates colocalization between green and red fluorescence. (B) Flow cytometry analysis of DC maturation induced by PMLC. (C) PMLC-induced IL-1β secretion by wild-type DCs and NALP3$^{-/-}$ KO DCs.**

in the lymph node, mice were injected with either soluble OVA-AF488 or the equivalent amount of encapsulated OVA-AF488. PBS was injected as a negative control. Two days post-injection, popliteal lymph nodes were dissected and analyzed by flow cytometry. As depicted in Figure 3D, delivering OVA in a particulate form strongly increased the percentage of DCs becoming OVA positive when compared to soluble OVA (22.0 *vs* 9.4%). Besides augmenting antigen targeting to DCs, PMLC-mediated antigen delivery also resulted in an increased antigen delivery to B cells (32.3 *vs* 5.7%) and macrophages (64.1 *vs* 29.8%). Moreover, PMLC-mediated antigen delivery increased not only the number of antigen-positive APCs but also the amount of antigen per APC as indicated by a strong increase in mean fluorescence intensity (Figure 3E).

To analyze whether this increased antigen delivery by PMLCs toward APCs also enhanced antigen presentation, naïve mice were intravenously injected with CFSE-labeled (*i.e.*, marked with an intracellular green fluorescent tracer) OT-I or OT-II cells. OT-I cells are CD8 T cells with a transgenic T cell receptor specifically recognizing the OVA peptide SIINFEKL presented by MHCI, while OT-II cells are transgenic CD4 T cells specifically recognizing the OVA peptide LSQAVHAAHAEINEAGR presented by MHCII.[51] Two days following injection with the CFSE-labeled OT-I or OT-II cells, mice were immunized with soluble OVA or the equivalent amount of encapsulated OVA. At days 2, 5, and 7 past immunization, draining lymph nodes were dissected and their cell content analyzed by FACS to monitor proliferation of the adoptively transferred OT-I and OT-II cells. Each time a transgenic T cell divides, the CFSE signal is diluted over the two daughter cells, resulting in a decrease in fluorescence intensity allowing close *ex vivo* monitoring of the proliferation of OVA-specific CD4 and CD8 T cells.

An overview of the experimental procedure is given in Figure 4A. The histograms in Figure 4B1,B2 are, respectively, gated onto CD8 and CD4 Vα2 Vβ5 positive T cells, representing the CFSE-labeled adoptively transferred transgenic OT-I and OT-II cells. Five days following immunization, a profound increase in OT-I proliferation was detectable in response to injection of the encapsulated OVA. The discrepancy between soluble OVA and encapsulated OVA in promoting MHCI-mediated presentation of OVA to OT-I cells became even more pronounced at day 7, with almost all OT-I cells having undergone 10 or more divisions (reaching the detection limit of the CFSE signal) when the OVA was administrated in the encapsulated form. OT-I proliferation in response to soluble OVA in contrast was far less potent and seemed to have halted already by day 5 post-injection. OT-II proliferation started off earlier in response to soluble OVA, with the first divisions already visible at day 2 post-injection. Five days post-immunization, however, OT-II cells from mice immunized with encapsulated OVA had already undergone slightly more divisions compared to those immunized with soluble OVA, a discrepancy that became even more pronounced at the day 7 interval. The delay in OT-II proliferation for encapsulated OVA is likely due to differences in the kinetics of OVA arriving and being presented in the draining lymph nodes, as soluble OVA can be passively drained with the interstitial fluid, while encapsulated OVA needs to be taken up by APCs and actively transported to the draining lymph nodes. Similar to OT-I, proliferation of OT-II in response to soluble OVA did not proceed further beyond day 5 after injection,

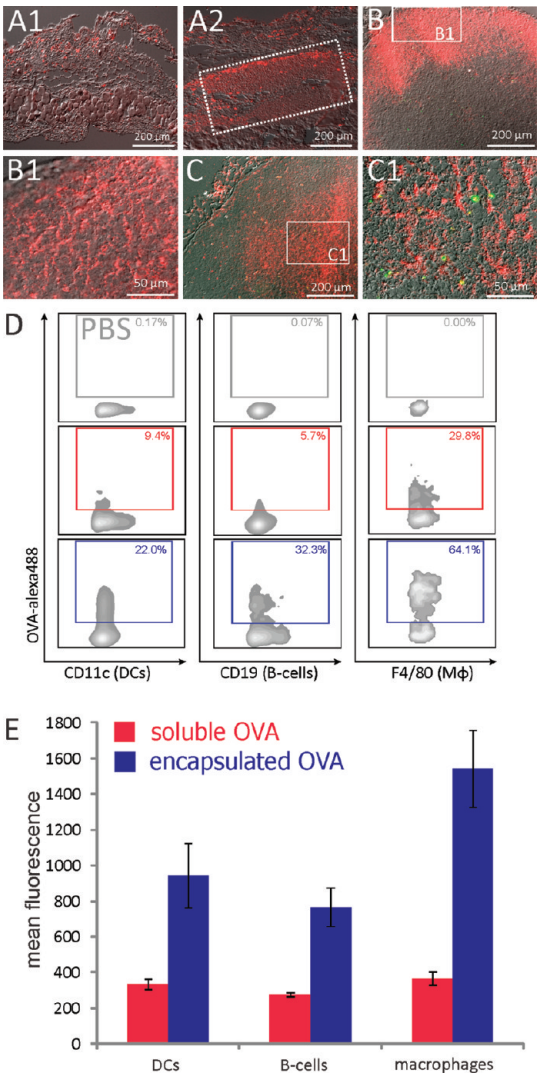

Figure 3. PMLC-mediated antigen delivery enhances antigen uptake. (A) Immunohistochemical staining of skin sections taken after subcutaneous injection of mice with PBS (A1) or capsules (A2). Antigen-presenting cells were stained for MHCII with the rat anti-mouse I-A/I-E antibody M5/114.15.2. Detection was performed using goat anti-rat AF555. (B,C) Immunohistochemical staining of cryosections taken from the draining lymph nodes 48 h after subcutaneous injection of PMLC loaded with OVA-AF488 (green fluorescence). In panels B, B cells were stained red fluorescent using the anti-mouse CD45R/B220 (RA-6B2) antibody and goat anti-rat AF555. In panels C, T cells were stained red fluorescent using rabbit anti-mouse anti-CD3 and goat anti-rabbit AF594. (D,E) Flow cytometric analysis of cells derived from the draining lymph nodes 48 h after injection of PBS (gray), soluble OVA-AF488 (red), or encapsulated OVA-AF488 (blue). Cells were stained with MHCII-eFluor to discern professional APCs and with CD11c-APC, CD19-PE, or F4/80-APC to identify, respectively, DCs, B cells, or macrophages. (E) Percentages of OVA-positive DCs, B cells, and macrophages following footpad injection of PBS, 5 μg of soluble OVA-AF488, and 5 μg of encapsulated OVA-AF488, and (E) mean intensity of green fluorescence of OVA-positive DCs, B cells, and macrophages following footpad injection of 5 μg of soluble or 5 μg of encapsulated OVA-AF488.

while in the case of encapsulated OVA, proliferation was still ongoing at day 7.

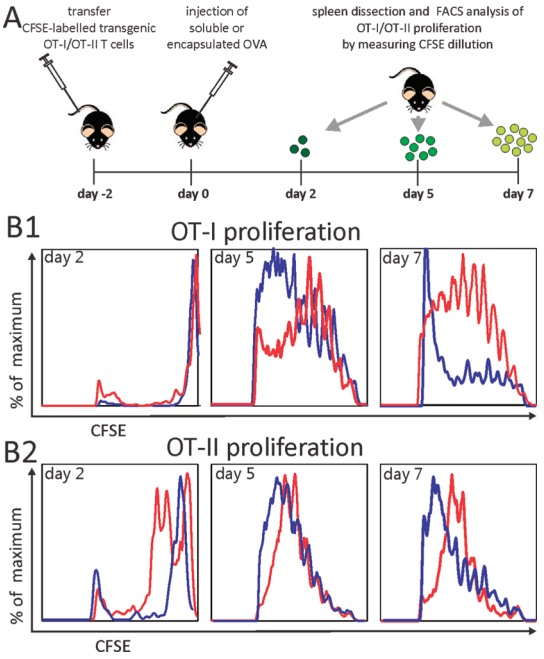

Figure 4. PMLC-mediated antigen delivery enhances antigen presentation. (A) Schematic representation of the experimental setup and (B1,B2) flow cytometric histograms showing OT-I and OT-II proliferation as a function of time after vaccination for mice vaccinated with either 50 μg of soluble or 50 μg of encapsulated OVA and following adoptive transfer of, respectively, CFSE-labeled OT-I and OT-II cells.

These data confirm and extend our previously reported *in vitro* findings, thereby clearly indicating that PMLCs have the capacity to enhance antigen presentation not only quantitatively but also qualitatively by preferentially stimulating cross-presentation and even increasing MHCII-mediated antigen presentation to CD4 T cells. This differs from other results on hollow capsules reported by the Caruso group which observed predominantly OT-II proliferation, while OT-I responses were only marginally upregulated.[24] Most likely, this is due to the different nature of the capsules which were assembled through hydrogen bonding and disulfide stabilization.

PMLC-Mediated Antigen Delivery Enhances Cellular Immunity. In a next series of experiments, we analyzed to what extent the increased antigen presentation mediated by PMLC was translated into the generation of more potent T cell responses. As depicted in Figure 5A, footpad injection of PMLC-encapsulated OVA resulted in increased numbers of T cells, CD4, as well as CD8 T cells, in the draining lymph nodes 1 week post-injection, indicative of ongoing T cell proliferation. The final goal of any vaccine is the induction of antigen-specific memory responses that offer over prolonged time the ability to react fast and vigorously against re-exposure to antigen upon infection. To assess this issue, we subcutaneously immunized naïve mice twice separated by a 3 week interval with either soluble or encapsulated OVA. To evaluate the induction of memory cellular immune responses by PMLC-based vaccination,

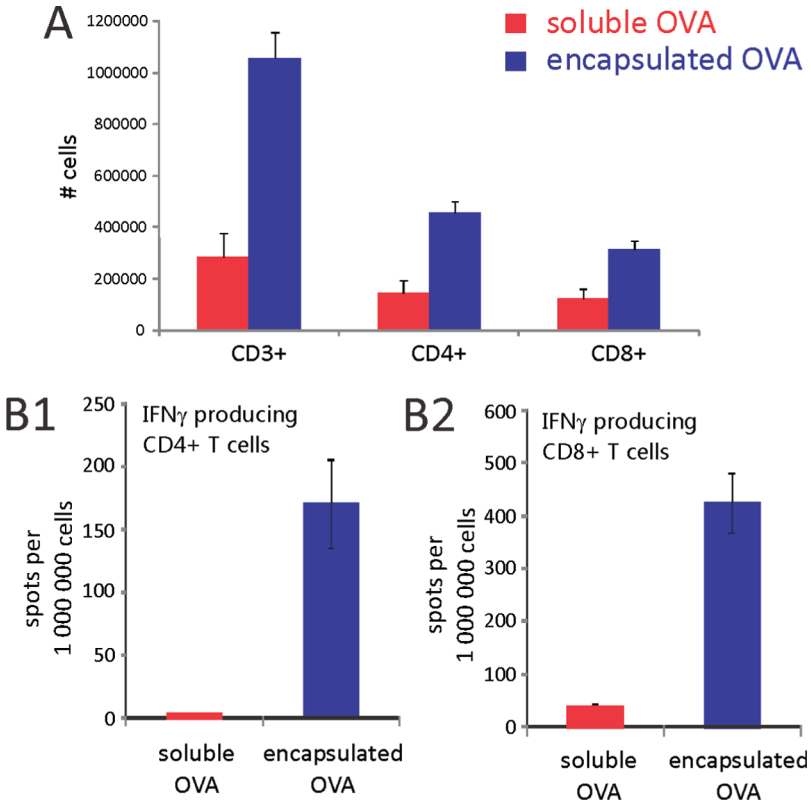

Figure 5. PMLC-mediated antigen delivery enhances cellular immunity. (A) Flow cytometric determination of total T cell, CD4, and CD8 T cell numbers in the draining popliteal lymph nodes 7 days post-footpad injection of either 5 μg of soluble or 5 μg of encapsulated OVA. (B) Induction of IFN-γ producing, OVA-specific CD4+ (B1), and CD8+ T cells (B2) as determined by ELISPOT.

splenocytes were prepared 3 weeks following the booster immunization and analyzed by ELISPOT following a 24 h *in vitro* restimulation with either the MHCI or MHCII peptide epitope of OVA. As depicted in Figure 5B1,B2, immunization with encapsulated OVA strongly boosted the numbers of OVA-specific IFN-γ secreting CD4 and CD8 T cells when compared to soluble antigen.

The functional relevance of these PMLC-provoked cellular immune responses was determined in a syngeneic C57BL/6 B16 melanoma model. For this purpose, we used an OVA-transduced B16 melanoma cell line, which can be recognized and killed by high avidity OVA-specific CD8 cytotoxic T cells.[52] Therefore, mice were subcutaneously immunized with OVA-loaded capsules or soluble OVA. Three weeks after the booster immunization, mice were challenged with 2×10^5 B16-OVA melanoma cells at their tail basis. Tumor growth was followed over time, and mice were euthanized when the mean tumor diameter exceeded 10 mm. An overview of the experimental procedure applied is given in Figure 6C1. As shown in Figure 6C2, mice immunized with soluble OVA failed to control tumor growth and rapidly had to be euthanized. Prophylactic vaccination with PMLC-encapsulated OVA in contrast strongly increased survival rates, with seven out of eight mice remaining free of visible tumors for at least 100 days post-tumor challenge.

PMLC-Mediated Antigen Delivery Enhances Humoral Immunity. For most of the vaccines available today, protection has been tightly linked to the induction of potent humoral immune responses.[53] As described earlier, PMLC-based antigen delivery not only promotes the induction of CD4 T cell responses that may provide help to B cells but also directly increases antigen delivery to B cells. To unravel to what extent PMLCs support the generation of more potent B cell responses, mice were immunized *via* the footpad with either soluble or PMLC-encapsulated OVA. One week after injection, draining popliteal lymph nodes were dissected and analyzed by FACS. As depicted in Figure 7A1,A2, PMLC-based immunization dramatically increased B cell numbers in the draining popliteal lymph nodes, indicative of ongoing B cell activation and proliferation. These increased B cell numbers coincided with a strong increase in germinal center (GC) B cells, which were almost totally absent following immunization with soluble antigen. Formation of germinal centers where activated B cells undergo somatic hypermutation leading to affinity maturation and isotype class switching is crucial for the generation of long living plasma cells and memory B cells and, consequently, a major goal of many vaccines.[54] Furthermore, PMLC-based immunization resulted in an over 10-fold increase in the number of antibody secreting plasma

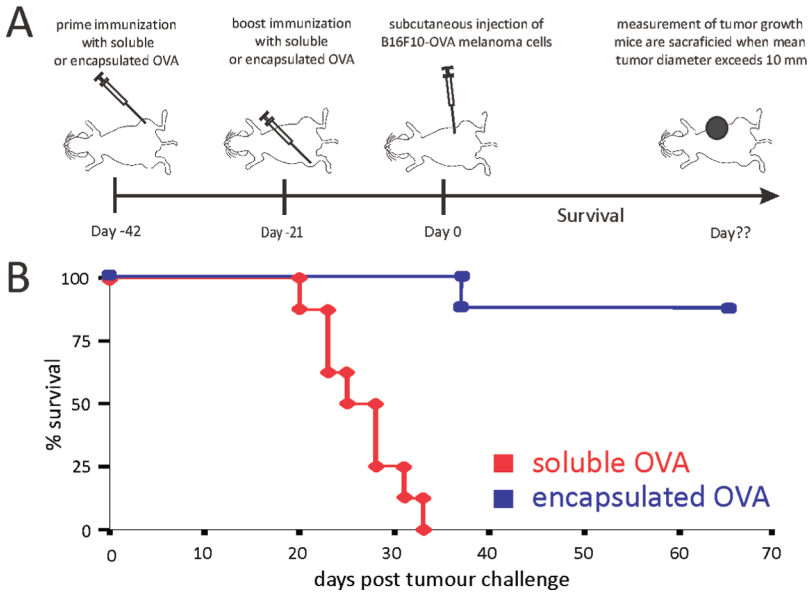

Figure 6. Tumor challenge. (A) Schematic outline of the experimental setup. (B) Survival of mice vaccinated with, respectively, 50 μg of soluble or 50 μg of encapsulated OVA, following inoculation (day 0) with B16-OVA melanoma.

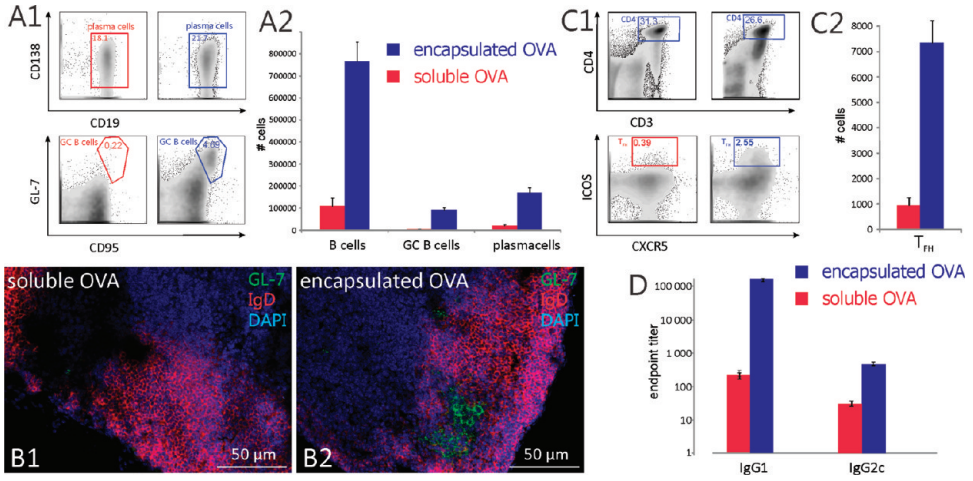

Figure 7. PMLC-mediated antigen delivery enhances humoral immunity. (A) Frequency (A1) and total numbers (A2) of B cells, germinal center (GC) B cells and plasma cells were determined by flow cytometry 7 days post-footpad injection of either 5 μg of soluble or 5 μg of encapsulated OVA. B cells were defined as CD45+ CD19+ CD3− cells, plasma cells as CD138+ B cells and GC B cells as CD138− GL-7+ CD95+ B cells. Frequencies shown in the dot plots are displayed as the frequencies of the parent gates. A detailed overview of the gating strategy is giving in Figure S1A of the Supporting Information. (B) Confocal analysis of germinal center formation on cryosections of popliteal lymph nodes 7 days post-footpad injection of 5 μg of soluble OVA (B1) or 5 μg of encapsulated OVA (B2). Cell nuclei were stained blue using DAPI, primary B cell follicles stained red using IgD-PE, and germinal center B cells green using GL7-FITC. (C) Frequencies (C1) and total numbers (C2) of CD4 T_{FH} cells were determined by flow cytometry 7 days following footpad injection of 5 μg of soluble or 5 μg of encapsulated OVA. T_{FH} cells were defined as CD3+ CD4+ T cells expressing ICOS and CXCR5. Frequencies of T_{FH} cells displayed in the dot plots are given as percentage of total CD3+ CD4+ T cells. A detailed overview of the gating strategy applied is given in Figure S1B of the Supporting Information. (D) Anti-OVA IgG1 and IgG2c titers as determined by ELISA 3 weeks following prime-booster immunization with each time 50 μg of soluble or 50 μg of encapsulated OVA.

cells. These observations were limited to the draining lymph nodes, as nondraining cervical lymph nodes showed no elevated B cell, GC B cells, and plasma cell numbers (Figure S1C, Supporting Information). The formation of germinal centers was also confirmed by confocal microscopy on cryosections of day 7 popliteal lymph nodes, clearly showing clusters of GL-7-positive cells in response to PMLC-based immunization (Figure 7B).

Full development of germinal centers requires T cells providing help to B cells. Recently, follicular T-helper (T_{FH}) cells have been identified as a new CD4 T-helper subset critically involved in supporting the germinal center reaction by providing help to B cells *via* cell−cell contact and cytokine secretion. These T_{FH} cells can be identified by their expression of ICOS and CXCR5.[55,56] Consequently, we analyzed draining popliteal lymph

nodes for the presence of T_{FH} by flow cytometry 7 days post-footpad immunization. As depicted in Figure 7C1,C2, PMLC-based immunization resulted in a vast increase in the number of T_{FH} cells, which were almost totally absent after immunization with soluble OVA. Again, the induction of T_{FH} responses was limited to the draining lymph node, as no increased T_{FH} responses could be observed in nondraining cervical lymph nodes (Figure S1C, Supporting Information).

Next, we determined to what extent the increased B cell responses following PMLC-based immunization augmented the antibody response. To this end, naïve mice received two immunizations with either soluble or encapsulated OVA, separated by a 3 week interval. Humoral responses were analyzed by ELISA on serum samples obtained 3 weeks following the booster immunization. As depicted in Figure 7D, antigen encapsulation increased OVA-specific IgG1 titers 100-fold while IgG2c titers were approximately 10-fold increased.

The functional relevance of the capacity of PMLC to promote humoral immune responses was tested in a murine influenza model using a recombinant influenza A virus M2e-fusion protein.[57] M2e is the ectodomain of the influenza M2 transmembrane protein, which functions as a proton-selective channel and has a vital function in the viral replication cycle.[58] In contrast to the hypervariable hemagglutinin, which is currently used as protective antigen in influenza vaccines, the M2e sequence is strongly conserved, making it an attractive candidate to develop a more universal influenza vaccine instead of today's seasonal flu vaccines that need to be adapted annually.[59] Protection mediated by M2e-based vaccination has been demonstrated to mainly rely on humoral immunity.[60] Because naturally M2e is presented as a tetrameric structure on the surface of influenza A virus-infected cells, De Filette *et al.* have fused M2e to a modified form of the leucine zipper derived from the yeast transcription factor GCN4, resulting in the generation of a soluble recombinant tetrameric protein, M2e-tGCN4.[57] Nevertheless, M2e-tGCN4 remains an intrinsically weak antigen requiring the addition of potent adjuvants to elicit protective antibody responses. M2e-tGCN4 was encapsulated inside PMLC, and Balb/c mice were immunized three times with either soluble or PMLC-encapsulated M2e-tGCN4. As a negative control, mice were immunized with either soluble or encapsulated BM2e-tGCN4 containing the ectodomain sequence of BM2, the counterpart of M2 in influenza B viruses. Earlier, it has been demonstrated that immunization with BM2e (Figure S2) fails to induce cross-reactive antibodies against M2e (influenza A).[57] One week after each immunization, serum was collected and M2e-specific antibody titers were determined by peptide ELISA. An overview of the experimental procedure is displayed in Figure 8A.

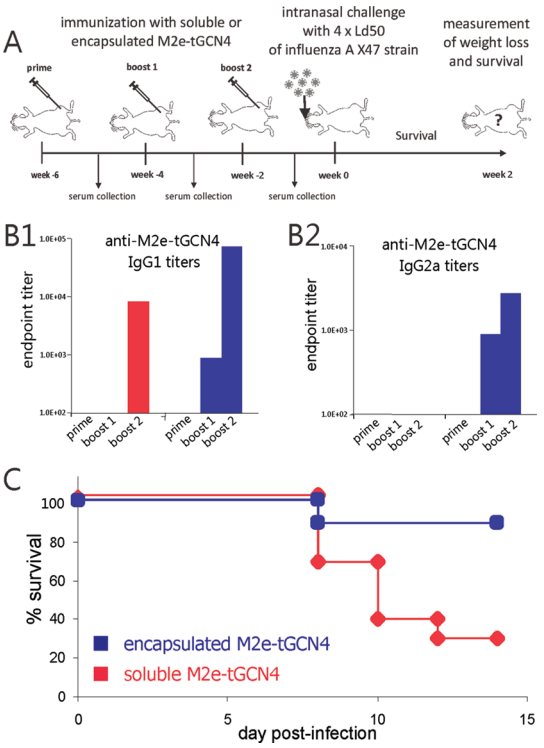

Figure 8. PMLC-mediated antigen delivery enhances protection against viral infection. (A) Schematic outline of the experimental setup. (B) Anti-M2e-tGCN4 IgG1 (B1) and anti-M2e-tGCN4 IgG2a (B2) titers determined after immunization with either 10 μg of soluble or 10 μg of encapsulated M2e-tGCN4. (C) Survival curves of soluble or encapsulated M2e-TGCN4 vaccinated mice challenged with 4 $\times$ LD_{50} of mouse-adapted influenza A virus X47.

As depicted in Figure 8B, immunization with encapsulated M2e-tGCN4 not only strongly increased anti-M2e IgG1 titers but also increased the speed of the observed response. Indeed, while antibodies against M2e were only detectable after two booster immunizations with soluble M2e-tGCN4, PMLC-encapsulated M2e-tGCN4 induced detectable anti-M2e titers already after a first booster immunization, which might be of significant benefit in case of flu pandemic. In addition, while immunization with soluble M2e-tGCN4 failed to generate detectable anti-M2e IgG2a antibody titers even after two booster immunizations, vaccination with encapsulated antigen was clearly capable of doing so, with anti-M2e IgG2a titers being detectable already after the first booster immunization. To address whether these PMLC-based humoral responses were robust enough to protect against influenza A, mice were challenged with a lethal dose (4 $\times$ LD_{50}) of mouse-adapted X47 virus and survival was followed over time. As expected, immunization with BM2e-tGCN4 did not result in significant survival, irrespective of antigen encapsulation (Figure S2, Supporting Information). Immunization with encapsulated M2e-tGCN4 in contrast provided a strong survival benefit compared to immunization with the soluble antigen, with 9 out of 10 mice surviving a lethal influenza A challenge (Figure 8C).

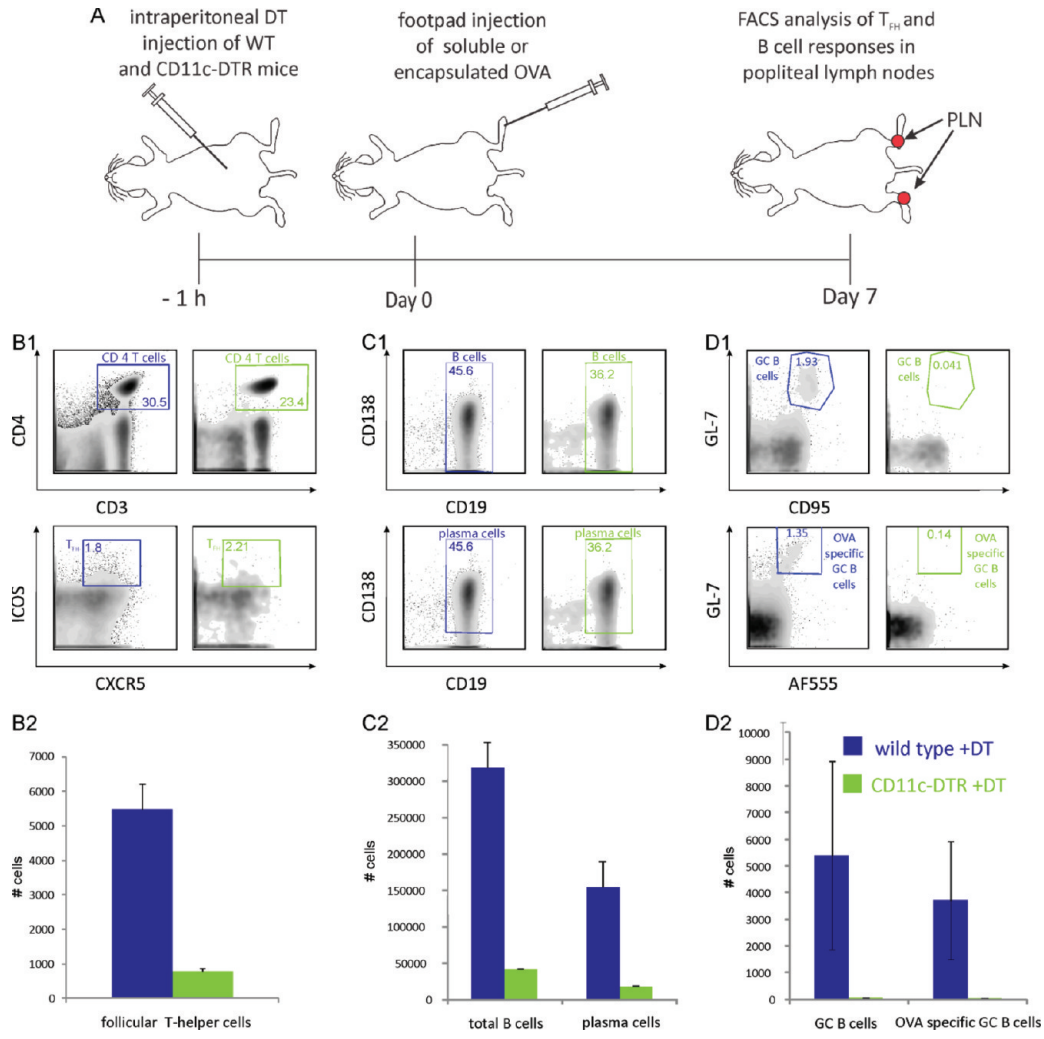

Figure 9. DCs are crucial mediators of PMLC-induced immunity. (A) To analyze the role of DCs in the PMLC-mediated immune response, CD11c-DTR mice were systemically depleted of CD11c^{hi} DCs by intraperitoneal of DT 1 h before footpad injection of either 5 μg of soluble or 5 μg of encapsulated OVA. As a control group, wild-type mice were also injected with the same amount of DT. Seven days post-injection, B and T_{FH} cell responses in draining lymph nodes were analyzed by flow cytometry. (B) Frequencies (B1) and total numbers (B2) of CD4 T_{FH} cells following injection of DT-injected WT (blue) and CD11c-DTR (green) mice with 5 μg of encapsulated OVA. T_{FH} cells were identified as CD3+CD4+ T cells expressing ICOS and CXCR5. (B1) Percentages displayed in the gates are expressed as percentage of the parent gate. Gating was performed as described in Figure S1B (Supporting Information). (C,D) Flow cytometric analysis of B cell responses following injection of DT-injected WT (blue) and CD11c-DTR (green) mice with 5 μg of encapsulated OVA. B cells were defined as CD45+ CD19+ CD3− cells, plasma cells as CD138+ B cells, and GC B cells as CD138− GL7+ CD95+B cells. OVA-specific GC B cells were further identified as GC-B cells binding OVA-AF555 by flow cytometry. Frequencies shown in the dot plots are displayed as the frequencies of the parent gates. Gating was performed as described in Figure S1A (Supporting Information).

DCs Are Crucial Mediators of PMLC-Induced Immunity. The above-described data demonstrate that PMLC-based antigen delivery has the capacity to potently increase B and T cell responses against encapsulated antigen. To unravel to what extent DCs are the main mediators of these effects, we used CD11c-DTR transgenic mice. These mice transgenically express the receptor for the diphtheria toxin controlled by the DC-specific promoter CD11c, thereby allowing a specific systemic depletion of DCs following diphtheria toxin (DT) injection.[61] One hour before footpad injection of PMLC-encapsulated OVA, DCs were depleted by intraperitoneal injection of DT. In a control group, nontransgenic mice were injected with DT. Injection of DT to these wild-type mice does not result in DC depletion. Seven days following immunization, T_{FH} and B cell responses were analyzed in draining lymph nodes. Figure 9A gives an overview of the experimental procedure applied. As described earlier, when compared to soluble OVA, injection of encapsulated OVA resulted in a vast increase in the number of CD4 T_{FH} cells in control mice (Figure S3, Supporting Information). DC-depleted mice in contrast exhibited largely reduced numbers of T_{FH}, demonstrating the crucial role of DCs in the initiation of CD4 T_{FH} responses (Figure 9B2). On the B cell level, immunization of control mice with encapsulated OVA resulted again in a strong elevation of total B cell, plasma cell, and

germinal center B cell numbers (Figure S3, Supporting Information). Importantly, the vast majority of these germinal center B cells were OVA-specific, as demonstrated by their binding of OVA-AF555 *via* flow cytometry (Figure 9D1, lower panel). Depletion of DCs, however, dramatically reduced B cell and plasma cell numbers and resulted in an almost total abrogation of germinal B cell responses (Figure 9C,D). Taken together, these data clearly establish DCs as the key players mediating the adjuvant properties of PMLC *in vivo*.

CONCLUSIONS

PMLC-mediated vaccination resulted in an efficient delivery of encapsulated antigen to DCs, B cells, and macrophages *in vivo*. This improved antigen delivery toward professional APCs augmented antigen presentation, especially enforcing MHCI-mediated antigen presentation to CD8 T cells. On the T cell level, PMLC supported the generation of potent CD8 cytotoxic T cell responses and CD4 Th1 responses against encapsulated antigen. This is of great interest for the development of therapeutic vaccines against cancer but also for prophylactic vaccination against insidious pathogens such as HIV, malaria, and tuberculosis. Furthermore, a profound increase in CD4 T_{FH} cell responses, crucial supporters of the germinal center reaction, was observed in response to PMLC-based immunization. On the level of the B cell response, PMLC promoted the formation of germinal centers and increased the number of plasma cells, resulting in elevated antibody titers following subcutaneous immunization. The functional relevance of these PMLC-evoked immune responses was subsequently validated in a murine influenza model and a melanoma model. On a mechanistic level, we have identified DCs as the key players of PMLC-mediated vaccine delivery. Although PMLCs do not induce upregulation of co-stimulatory markers following uptake by bone marrow derived DCs *in vitro*, they activated the NALP3 inflammasome, a feature shared in common with several other particulates. Activation of the NALP inflammasome results in the release of the potent pro-inflammatory cytokine IL-1β, which might contribute to the observed inflammatory response following microcapsule injection. Whether and to what extent NALP3 inflammasome activation also contributes to the adaptive immune response following microparticulate antigen delivery currently constitutes a matter of intense scientific controversy.

MATERIALS AND METHODS

Polyelectrolyte Capsules. Calcium chloride ($CaCl_2$), sodium carbonate (Na_2CO_3), ovalbumin (OVA; grade VII), dextran sulfate (10 kDa), and poly-L-arginine hydrochloride (M_w > 70 kDa) were purchased from Sigma-Aldrich. Alexa Fluor 488 (AF488)-conjugated ovalbumin (OVA-AF488) and Alexa Fluor 555 (AF555)-conjugated ovalbumin (OVA-AF555) were purchased from Invitrogen. Phosphate buffered saline (PBS) was obtained from Gibco. M2e-tGCN4 was produced as earlier reported.[57]

Calcium carbonate ($CaCO_3$) microparticles were synthesized by addition of 0.625 mL of $CaCl_2$ (1 M) and 0.625 mL of Na_2CO_3 (1 M) to 5 mL of deionized water containing 1 mg of antigen (either OVA or M2e-tGCN4) under vigorous stirring. Laser diffraction (Malvern Mastersizer 2000) indicated a mean particle diameter of 3 μm. The obtained Ca_2CO_3 microparticles were subsequently centrifuged (3 min at 300*g*) and coated by dispersing them in 5 mL of a 2 mg/mL dextran sulfate solution containing 0.5 M NaCl. Importantly, to avoid particle aggregation, the centrifuged pellet was vortexed every time after decantation of the supernatant, prior to the addition of polyelectrolyte. Subsequently, the microparticles were collected by centrifugation (3 min at 300*g*), and residual dextran sulfate was removed by washing twice with deionized water. Microparticles were stirred in 5 mL of a 1 mg/mL poly-L-arginine solution in 0.5 M NaCl, centrifuged, and washed twice again. This procedure was repeated until two bilayers of dextran sulfate/poly-L-arginine were deposited. Hollow capsules were obtained by removing the $CaCO_3$ with an aqueous 0.2 M EDTA solution. The resulting capsules were washed twice with PBS, by centrifugation during 10 min at 1000 g and resuspended in 1 mL PBS. The capsule concentration was determined by hemocytometry to by 700 $\times$ 10^6 capsules/mL, and LPS concentrations were measured to be <1 EU/mL *via* the LAL assay. Zeta-potential measurements during capsule assembly were performed in distilled water on a Malvern Nanosizer ZS.

To measure antigen encapsulation, the supernatants obtained after each centrifugation step were collected and measured for their protein content using a Quick Start Bradford protein assay. When subtracted from the initial amount of antigen, an encapsulation efficiency of 51.4% for OVA and 48.6% for M2e-tGCN4 was calculated. The thus obtained capsule suspensions had an antigen concentration of approximately 0.5 mg/mL.

Microscopy. Confocal microscopy images were recorded on a Leica SP5 confocal microscope equipped with a 63$\times$ oil immersion objective. Scanning electron microscopy (SEM) images of gold-sputtered capsules that were dried from deionized water (to avoid recrystallization of PBS salts) onto a silicon wafer were recorded on a Quanta FEG FEI 200 scanning electron microscope. Transmission electron microscopy (TEM) images were recorded on a JEOL 1010 transmission electron microscope. Sample preparation was performed by fixing the capsules in 4% paraformaldehyde and 2.5% glutaraldehyde in 0.1 M Na cacodylate buffer (pH 7.2) for 4 h at room temperature followed by fixation overnight at 48 °C. After being washed three times for 20 min with buffer solution, cells were dehydrated through a graded ethanol series, including a bulk staining with 1% uranyl acetate at the 50% ethanol step followed by embedding in Spurr's resin. Ultrathin sections of a gold interference color were cut using an ultramicrotome (ultracut E/Reichert-Jung), followed by a post-staining with uranyl acetate and lead citrate in a Leica ultrastainer, and collected on Formvar-coated copper slot grids. They were viewed with a transmission electron microscope 1010 (JEOL, Tokyo, Japan).

Mice. C57BL/6 mice were obtained from Janvier. Balb/c mice, OT-I, and OT-II transgenic mice (C57BL/6) were purchased from Charles River. NALP3$^{-/-}$ and CD11c-DTR mice were bred in house. Mice were housed under specific pathogen-free conditions. All animal experiments were approved by the Local Ethical Committee of Ghent University.

DC Maturation Assay. To analyze the effects of PEM on the DC maturation status, day 8 bone marrow derived DCs (10^6/mL) were incubated with 5 μL/mL of empty polyelectrolyte microcapsules for 18 h. As a positive control for DC maturation, DCs were incubated with 100 ng/mL LPS (Sigma Aldrich). Cells were subsequently stained with Fc block (BD Pharmingen), MHCII-eFluor (eBioscience), CD11c-APC (BD Pharmingen), and either CD40-PE or CD86-PE (all BD Pharmingen) and analyzed by flow cytometry (LSRII Becton Dickinson).

IL-1β Assay. To address the capacity of polyelectrolyte microcapsules to activate the NALP inflammasome and trigger IL-1β release, bone marrow derived DCs were incubated with a dilution series of polyelectrolyte microcapsules (100-25-5-1 μL) either alone or in combination with a low dose of LPS (10 ng/mL) for 18 h. As negative controls, DCs prepared from NALP3$^{-/-}$ mice were incubated with the same concentrations of capsules and LPS. Following this incubation period, supernatant of the cultures was harvested and the amount of IL-1β released was measured by ELISA (BD Biosciences).

Immunohistochemistry. To assess the recruitment of antigen-presenting cells, mice were subcutaneously vaccinated with 100 μL capsule suspension containing 50 μg of OVA. Two days post-vaccination, the injection spot was dissected and fixed in 4% paraformaldehyde. Five micrometer thick paraffin sections were cut and stained with rat anti-mouse antibody M5/114 (BD Pharmingen) and goat anti-rat IgG-AF555 (Invitrogen) as a detection antibody.

To assess capsule transport to the draining lymph nodes, mice were vaccinated in the footpad with 10 μL capsule suspension containing 5 μg of OVA-AF488. Draining popliteal lymph nodes were dissected and frozen in mold containing OCT medium. Five micrometer cryosections were prepared and fixed with ice-cold action for 10 min, air-dried, and stored at -80 °C. Sections were fluorescently stained with either anti-mouse CD45R/B220 (RA-6B2, BD Pharmingen) and goat anti-rat Alexa Fluor 555 (Molecular Probes) to visualize the B cell area, or with rabbit anti-mouse anti-CD3 (Abcam 5690-100) and goat anti-rabbit Alexa Fluor 594 (Molecular Probes) to visualize the T cell zone.

For analysis of germinal center formation, mice were vaccinated in the footpad with 10 μL capsule suspension containing 5 μg of OVA-AF488. Sections of the draining popliteal lymph nodes were stained with IgD-PE and GL-7-FITC (both BD Pharmingen). DAPI was applied to visualize the nuclei. Subsequently, slides were mounted using Vectashield mounting medium (Vector Laboratories, Inc.) and examined by confocal microscopy.

Antigen Targeting to Lymph Node APCs. Antigen targeting to lymph node APCs was evaluated by flow cytometry using the following antibodies: MHCII-eFluor (ebioscience), CD11c-APC, CD19-PE, and F4/80-APC (all BD Pharmingen). Forty-eight hours following footpad injection of 10 μL containing 5 μg of either soluble or encapsulated OVA-AF488, popliteal lymph nodes were dissected and incubated for 30 min at 37 °C in RPMI medium (Invitrogen) containing 150 U/mL collagenase II (Sigma) to prepare single cell suspensions. Subsequently, cells were stained with MHCII-eFluor, CD19-PE, and CD11c-APC to discriminate B cells and DCs and with MHC-II-eFluor and F4/80-APC to visualize macrophages.

***In Vivo* OT-I and OT-II Proliferation.** OT-I or OT-II cells were purified from spleens by using the CD8 isolation kit II (Miltenyi) or CD4 isolation kit II (Milenyi), respectively, and labeled with the green fluorescent dye CFSE. Briefly, cells were incubated at a density of 10 $\times$ 106/mL in CFSE (5 μM) for 10 min at 37 °C. Staining was stopped by adding five volumes of ice-cold RPMI (Gibco) containing 10% FCS. After washing, 4 $\times$ 10^6 OT-I or OT-II cells were injected i.v. into the tail vain of sex-matched C57BL/6 mice. Two days following adoptive transfer of the CFSE-labeled OT cells, mice were subcutaneously immunized with 100 μL containing 50 μg of either soluble OVA or encapsulated OVA. Draining lymph nodes were harvested at days 2, 5, and 7 post-immunization. Single cell suspensions were prepared; cells were stained with anti-mouse Vβ5 (MR9-4)-biotin, anti-mouse Vα2 (B20.1)-PE, streptavidin-APC, and CD8a-PerCP or CD4aPerCP (all BD Pharmingen), and OT proliferation was analyzed on a LSRII flow cytometer.

T Cell Flow Cytometry. To determine the number of CD4 and CD8 T cells in the draining lymph nodes, mice were immunized *via* the footpad with either 5 μg of soluble or encapsulated OVA. One week following injection, popliteal lymph nodes were dissected and single cell suspensions prepared as described previously. Cells were stained with CD3-AF488, CD4-PerCP, and CD8-FITC (all BD Pharmingen) to discriminate CD4 and CD8 T cells and analyzed by flow cytometry (LSRII Becton Dickinson).

ELISPOT. To analyze the number of IFN-γ secreting T cells, spleen from mice immunized with either 50 μg of soluble or encapsulated OVA were dissected 3 weeks following the booster immunization. Single cells suspensions were prepared and red blood cells lysed using ACK red blood cell lysis buffer (BioWhittaker). Splenocytes were subsequently restimulated with either 5 μg/mL SIINFEKL peptide (MHCI epitope of OVA) or 5 μg/mL SQAVHAAHAEINEAGR peptide (MHCII epitope of OVA). Following this *in vitro* restimulation period, 2.5 $\times$ 10^5 splenocytes were incubated on ELISPOT plates precoated with IFN-γ capture antibody (Diaclone) for another 24 h in the presence of either 5 μg/mL SIINFEKL or SQAVHAAHAEINEAGR (Anaspec). Following this incubation period, ELISPOTs were analyzed according to the manufacturer's instructions.

Tumor Challenge. The OVA-transfected melanoma cell line B16 (B16-OVA) was kindly provided by Prof. Dr. Y. Van Kooyk (University of Amsterdam, The Netherlads). Prior to tumor challenge, mice were vaccinated two times with a 3 week interval with 100 μL containing 50 μg of either soluble OVA or encapsulated OVA. Three weeks following the last immunization, mice were challenged subcutaneously with 2 $\times$ 10^5 B16-OVA melanoma cells. Tumor growth was followed over time, and mice were euthanized when the mean tumor diameter exceeded 10 mm.

B Cell and CD4 T$_{FH}$ Multicolour Flow Cytometry. To analyze B and CD4 TFH responses, the following antibodies were used: CD45 PE-TxRed (Invitrogen), CD95-PE-Cy7, GL7-FITC, CXCR5-biotin, CD138-APC, CD19-APC-Cy7 (all BD Pharmingen), ICOS-PE-cy5, streptavidin-PE-Cy7, CD4-APC, and CD3-AF700 (all EBioscience). Mice were vaccinated in the footpad with 10 μL containing 5 μg of either soluble or encapsulated OVA. Single cell suspensions of the draining popliteal lymph nodes were prepared 7 days post-footpad injection. Cell suspensions were stained with CD45-PE-TxRed, CD19-APC-Cy7, CD138-APC, GL7-FITC, and CD95-PE-Cy7 to identify B cells, plasma cells, and GC B cells. CD4 TFH cells were identified using CD3-AF700, CD4-APC, ICOS-PE-Cy5, CXCR5-biotin, and streptavidin-PE-Cy7. To gate out dead cells, cell suspensions were subsequently stained with Aqua (Invitrogen) in PBS.

Detection of Antibody Titers in Serum Against OVA. Mice were vaccinated twice with a 2 week interval with 100 μL containing 50 μg of either soluble or encapsulated OVA. For the detection of anti-OVA antibodies, blood samples were collected from the ventral tail vein and serum was prepared overnight at 4 °C. Maxisorp (Nunc) plates were coated overnight at 4 °C with OVA (10 μg/mL) and incubated with serial dilutions of serum. ELISAs were subsequently detected with, respectively, goat anti-mouse IgG1-HRP (Southern Biotech) and goat anti-mouse IgG2c-HRP (Cellab).

Detection of Antibody Titers in Serum Against M2e and Influenza A Virus Challenge. BALB/c mice were vaccinated three times with a 2 week interval with 100 μL containing 10 μg of either soluble or encapsulated M2e-tGNC4. The M2e peptide ELISA was performed as described previously.[57] Two weeks after each immunization, blood samples were collected. The titers of M2e-specific antibodies in the prepared serum of each mouse IgG subclass were determined by a M2e-peptide ELISA. Briefly, microtiter plates (Maxisorp, Nunc) were coated with M2e/peptide solution in sodium bicarbonate buffer, pH 9.7, and incubated overnight at 37 °C. After blocking, serum samples were loaded on the peptide-coated plates. Detection was performed using peroxidase-labeled antibodies directed against mouse IgG1 or IgG2a (Southern Biotechnology Associates, Inc.), followed by incubation with the peroxidase substrate tetramethylbenzidine (Sigma–Aldrich). The reaction was stopped by adding 1 M H_2SO_4, and the absorbance was measured at 450 nm. Two weeks after the last immunization, mice were anesthetized with isoflurane and challenged by intranasal administration of 50 μL PBS containing four LD50 of mouse-adapted X47 (PR8 3 A/Victoria/3/75) virus. Following challenge, survival and body weight were monitored daily for 14 days. Loss of 25% of body weight was used as the end point for euthanizing moribund mice.

***In Vivo* DC Depletion.** To evaluate the role of DCs in the PMLC-mediated immune response, CD11c^{hi} DCs were depleted 1 h before injection of soluble or encapsulated OVA by intraperitoneal injection of DT (50 ng).

Conflict of Interest: The authors declare no competing financial interest.

Acknowledgment. This research was supported by the Ghent University through a Methusalem BOF09/01M00709

Grant. B.G.D.G. acknowledges the FWO-Flanders for a postdoctoral scholarship and Ghent University (BOF-GOA) for funding. S.D.K. acknowledges Ghent University (BOF) for funding. C.P. acknowledges the ITG (SOFI) for a Ph.D. scholarship.

Supporting Information Available: Additional experimental details. This material is available free of charge *via* the Internet at http://pubs.acs.org.

REFERENCES AND NOTES

1. Querec, T.; Bennouna, S.; Alkan, S.; Laouar, Y.; Gorden, K.; Flavell, R.; Akira, S.; Ahmed, R.; Pulendran, B. Yellow Fever Vaccine YF-17D Activates Multiple Dendritic Cell Subsets *via* TLR2, 7, 8, and 9 To Stimulate Polyvalent Immunity. *J. Exp. Med.* **2006**, *203*, 413–424.
2. Plotkin, S. A. Vaccines: Past, Present and Future. *Nat. Med.* **2005**, *11*, S5–S11.
3. Rappuoli, R. From Pasteur to Genomics: Progress and Challenges in Infectious Diseases. *Nat. Med.* **2004**, *10*, 1177–1185.
4. Ellner, J. J.; Hirsch, C. S.; Whalen, C. C. Correlates of Protective Immunity to *Mycobacterium tuberculosis* in Humans. *Clin. Infect. Dis.* **2000**, *30*, S279–S282.
5. Walker, B. D.; Burton, D. R. Toward an AIDS Vaccine. *Science* **2008**, *320*, 760–764.
6. Lonchay, C.; van der Bruggen, P.; Connerotte, T.; Hanagiri, T.; Coulie, P.; Colau, D.; Lucas, S.; Van Pel, A.; Thielemans, K.; van Baren, N.; *et al.* Correlation between Tumor Regression and T Cell Responses in Melanoma Patients Vaccinated with a MAGE Antigen. *Proc. Natl. Acad. Sci. U.S.A.* **2004**, *101*, 14631–14638.
7. Dezfouli, S.; Hatzinisiriou, I.; Ralph, S. J. Enhancing CTL Responses to Melanoma Cell Vaccines *in Vivo*: Synergistic Increases Obtained Using IFNγ Primed and IFNβ Treated B7−1(+)B16-F10 Melanoma Cells. *Immunol. Cell Biol.* **2003**, *81*, 459–471.
8. Reed, S. G.; Bertholet, S.; Coler, R. N.; Friede, M. New Horizons in Adjuvants for Vaccine Development. *Trends Immunol.* **2009**, *30*, 23–32.
9. Seubert, A.; Monaci, E.; Pizza, M.; O'Hagan, D. T.; Wack, A. The Adjuvants Aluminum Hydroxide and MF59 Induce Monocyte and Granulocyte Chemoattractants and Enhance Monocyte Differentiation toward Dendritic Cells. *J. Immunol.* **2008**, *180*, 5402–5412.
10. Lambrecht, B. N.; Kool, M.; Willart, M. A. M.; Hammad, H. Mechanism of Action of Clinically Approved Adjuvants. *Curr. Opin. Immunol.* **2009**, *21*, 23–29.
11. Coffman, R. L.; Sher, A.; Seder, R. A. Vaccine Adjuvants: Putting Innate Immunity to Work. *Immunity* **2010**, *33*, 492–503.
12. Reddy, S. T.; van der Vlies, A. J.; Simeoni, E.; Angeli, V.; Randolph, G. J.; O'Neil, C. P.; Lee, L. K.; Swartz, M. A.; Hubbell, J. A. Exploiting Lymphatic Transport and Complement Activation in Nanoparticle Vaccines. *Nat. Biotechnol.* **2007**, *25*, 1159–1164.
13. Kwon, Y. J.; James, E.; Shastri, N.; Frechet, J. M. J. *In Vivo* Targeting of Dendritic Cells for Activation of Cellular Immunity Using Vaccine Carriers Based on pH-Responsive Microparticles. *Proc. Natl. Acad. Sci. U.S.A.* **2005**, *102*, 18264–18268.
14. Moon, J. J.; Suh, H.; Bershteyn, A.; Stephan, M. T.; Liu, H.; Huang, B.; Sohail, M.; Luo, S.; Um, S. H.; Khant, H.; *et al.* Interbilayer-Crosslinked Multilamellar Vesicles as Synthetic Vaccines for Potent Humoral and Cellular Immune Responses. *Nat. Mater.* **2011**, *10*, 243–251.
15. Kasturi, S. P.; Skountzou, I.; Albrecht, R. A.; Koutsonanos, D.; Hua, T.; Nakaya, H. I.; Ravindran, R.; Stewart, S.; Alam, M.; Kwissa, M.; *et al.* Programming the Magnitude and Persistence of Antibody Responses with Innate Immunity. *Nature* **2011**, *470*, 543–547.
16. De Koker, S.; Lambrecht, B. N.; Willart, M. A.; van Kooyk, Y.; Grooten, J.; Vervaet, C.; Remon, J. P.; De Geest, B. G. Designing Polymeric Particles for Antigen Delivery. *Chem. Soc. Rev.* **2011**, *40*, 320–339.
17. Qi, H.; Egen, J. G.; Huang, A. Y. C.; Germain, R. N. Extrafollicular Activation of Lymph Node B Cells by Antigen-Bearing Dendritic Cells. *Science* **2006**, *312*, 1672–1676.
18. Donath, E.; Sukhorukov, G. B.; Caruso, F.; Davis, S. A.; Mohwald, H. Novel Hollow Polymer Shells by Colloid-Templated Assembly of Polyelectrolytes. *Angew. Chem., Int. Ed.* **1998**, *37*, 2202–2205.
19. Caruso, F.; Caruso, R. A.; Mohwald, H. Nanoengineering of Inorganic and Hybrid Hollow Spheres by Colloidal Templating. *Science* **1998**, *282*, 1111–1114.
20. De Geest, B. G.; Sanders, N. N.; Sukhorukov, G. B.; Demeester, J.; De Smedt, S. C. Release Mechanisms for Polyelectrolyte Capsules. *Chem. Soc. Rev.* **2007**, *36*, 636–649.
21. Quinn, J. F.; Johnston, A. P. R; Such, G. K.; Zelikin, A. N.; Caruso, F. Next Generation, Sequentially Assembled Ultrathin Films: Beyond Electrostatics. *Chem. Soc. Rev.* **2007**, *36*, 707–718.
22. De Rose, R.; Zelikin, A. N.; Johnston, A. P. R; Sexton, A.; Chong, S.-F.; Cortez, C.; Mulholland, W.; Caruso, F.; Kent, S. J. Binding, Internalization, and Antigen Presentation of Vaccine-Loaded Nanoengineered Capsules in Blood. *Adv. Mater.* **2008**, *20*, 4698–4703.
23. De Koker, S.; De Geest, B. G.; Singh, S. K.; De Rycke, R.; Naessens, T.; Van Kooyk, Y.; Demeester, J.; De Smedt, S. C.; Grooten, J. Polyelectrolyte Microcapsules as Antigen Delivery Vehicles to Dendritic Cells: Uptake, Processing, and Cross-Presentation of Encapsulated Antigens. *Angew. Chem., Int. Ed.* **2009**, *48*, 8485–8489.
24. Sexton, A.; Whitney, P. G.; Chong, S.-F.; Zelikin, A. N.; Johnston, A. P. R; De Rose, R.; Brooks, A. G.; Caruso, F.; Kent, S. J. A Protective Vaccine Delivery System for *In Vivo* T Cell Stimulation Using Nanoengineered Polymer Hydrogel Capsules. *ACS Nano* **2009**, *3*, 3391–3400.
25. De Koker, S.; Naessens, T.; De Geest, B. G.; Bogaert, P.; Demeester, J.; De Smedt, S.; Grooten, J. Biodegradable Polyelectrolyte Microcapsules: Antigen Delivery Tools with Th17 Skewing Activity after Pulmonary Delivery. *J. Immunol.* **2010**, *184*, 203–211.
26. Volodkin, D. V.; Larionova, N. I.; Sukhorukov, G. B. Protein Encapsulation *via* Porous $CaCO_3$ Microparticles Templating. *Biomacromolecules* **2004**, *5*, 1962–1972.
27. Yu, A. M.; Wang, Y. J.; Barlow, E.; Caruso, F. Mesoporous Silica Particles as Templates for Preparing Enzyme-Loaded Biocompatible Microcapsules. *Adv. Mater.* **2005**, *17*, 1737–1741.
28. Decher, G. Fuzzy Nanoassemblies: Toward Layered Polymeric Multicomposites. *Science* **1997**, *277*, 1232–1237.
29. Rivera-Gil, P.; De Koker, S.; De Geest, B. G.; Parak, W. J. Intracellular Processing of Proteins Mediated by Biodegradable Polyelectrolyte Capsules. *Nano Lett.* **2009**, *9*, 4398–4402.
30. De Geest, B. G.; Vandenbroucke, R. E.; Guenther, A. M.; Sukhorukov, G. B.; Hennink, W. E.; Sanders, N. N.; Demeester, J.; De Smedt, S. C. Intracellularly Degradable Polyelectrolyte Microcapsules. *Adv. Mater.* **2006**, *18*, 1005–1009.
31. De Koker, S.; De Geest, B. G.; Cuvelier, C.; Ferdinande, L.; Deckers, W.; Hennink, W. E.; De Smedt, S.; Mertens, N. *In Vivo* Cellular Uptake, Degradation, and Biocompatibility of Polyelectrolyte Microcapsules. *Adv. Funct. Mater.* **2007**, *17*, 3754–3763.
32. Harris, J.; Sharp, F. A.; Lavelle, E. C. The Role of Inflammasomes in the Immunostimulatory Effects of Particulate Vaccine Adjuvants. *Eur. J. Immunol.* **2010**, *40*, 634–638.
33. Petrov, A. I.; Volodkin, D. V.; Sukhorukov, G. B. Protein-Calcium Carbonate Coprecipitation: A Tool for Protein Encapsulation. *Biotechnol. Prog.* **2005**, *21*, 918–925.
34. De Cock, L. J.; Lenoir, J.; De Koker, S.; Vermeersch, V.; Skirtach, A. G.; Dubruel, P.; Adriaens, E.; Vervaet, C.; Remon, J. P.; De Geest, B. G. Mucosal Irritation Potential of Polyelectrolyte Multilayer Capsules. *Biomaterials* **2011**, *32*, 1967–1977.
35. De Geest, B. G.; Dejugnat, C.; Prevot, M.; Sukhorukov, G. B.; Demeester, J.; De Smedt, S. C. Self-Rupturing and Hollow Microcapsules Prepared from Bio-Polyelectrolyte-Coated Microgels. *Adv. Funct. Mater.* **2007**, *17*, 531–537.

36. De Geest, B. G.; Dejugnat, C.; Sukhorukov, G. B.; Braeckmans, K.; De Smedt, S. C.; Demeester, J. Self-Rupturing Microcapsules. *Adv. Mater.* **2005**, *17*, 2357–2361.
37. De Geest, B. G.; De Koker, S.; Immesoete, K.; Demeester, J.; De Smedt, S. C.; Hennink, W. E. Self-Exploding Beads Releasing Microcarriers. *Adv. Mater.* **2008**, *20*, 3687–3691.
38. De Geest, B. G.; McShane, M. J.; Demeester, J.; De Smedt, S. C.; Hennink, W. E. Microcapsules Ejecting Nanosized Species into the Environment. *J. Am. Chem. Soc.* **2008**, *130*, 14480–14482.
39. Szarpak, A.; Cui, D.; Dubreuil, F.; De Geest, B. G.; De Cock, L. J.; Picart, C.; Auzely-Velty, R. Designing Hyaluronic Acid-based Layer-by-Layer Capsules as a Carrier for Intracellular Drug Delivery. *Biomacromolecules* **2010**, *11*, 713–720.
40. Haynie, D. T.; Palath, N.; Liu, Y.; Li, B. Y.; Pargaonkar, N. Biomimetic Nanostructured Materials: Inherent Reversible Stabilization of Polypeptide Microcapsules. *Langmuir* **2005**, *21*, 1136–1138.
41. Borodina, T.; Markvicheva, E.; Kunizhev, S.; Moehwald, H.; Sukhorukov, G. B.; Kreft, O. Controlled Release of DNA from Self-Degrading Microcapsules. *Macromol. Rapid Commun.* **2007**, *28*, 1894–1899.
42. Ibarz, G.; Dahne, L.; Donath, E.; Mohwald, H. Smart Micro- and Nanocontainers for Storage, Transport, and Release. *Adv. Mater.* **2001**, *13*, 1324–1327.
43. Dejugnat, C.; Sukhorukov, G. B. pH-Responsive Properties of Hollow Polyelectrolyte Microcapsules Templated on Various Cores. *Langmuir* **2004**, *20*, 7265–7269.
44. Kang, J.; Dahne, L. Strong Response of Multilayer Polyelectrolyte Films to Cationic Surfactants. *Langmuir* **2011**, *27*, 4627–4634.
45. She, Z.; Antipina, M. N.; Li, J.; Sukhorukov, G. B. Mechanism of Protein Release from Polyelectrolyte Multilayer Microcapsules. *Biomacromolecules* **2010**, *11*, 1241–1247.
46. Dierendonck, M.; De Koker, S.; Cuvelier, C.; Grooten, J.; Vervaet, C.; Remon, J. P.; De Geest, B. G. Facile Two-Step Synthesis of Porous Antigen-Loaded Degradable Polyelectrolyte Microspheres. *Angew. Chem., Int. Ed.* **2010**, *49*, 8620–8624.
47. Dierendonck, M.; De Koker, S.; De Rycke, R.; Bogaert, P.; Grooten, J.; Vervaet, C.; Remon, J. P.; De Geest, B. G. Single-Step Formation of Degradable Intracellular Biomolecule Microreactors. *ACS Nano* **2011**, *5*, 6886–6893.
48. Reddy, S. T.; Swartz, M. A.; Hubbell, J. A. Targeting Dendritic Cells with Biomaterials: Developing the Next Generation of Vaccines. *Trends Immunol.* **2006**, *27*, 573–579.
49. Houde, M.; Bertholet, S.; Gagnon, E.; Brunet, S.; Goyette, G.; Laplante, A.; Princiotta, M. F.; Thibault, P.; Sacks, D.; Desjardins, M. Phagosomes Are Competent Organelles for Antigen Cross-Presentation. *Nature* **2003**, *425*, 402–406.
50. Fischer, S.; Uetz-von Allmen, E.; Waeckerle-Men, Y.; Groettrup, M.; Merkle, H. P.; Gander, B. The Preservation of Phenotype and Functionality of Dendritic Cells upon Phagocytosis of Polyelectrolyte-Coated PLGA Microparticles. *Biomaterials* **2007**, *28*, 994–1004.
51. Hogquist, K. A.; Jameson, S. C.; Heath, W. R.; Howard, J. L.; Bevan, M. J.; Carbone, F. R. T-Cell Receptor Antagonist Peptides Induce Positive Selection. *Cell* **1994**, *76*, 17–27.
52. Radford, K. J.; Higgins, D. E.; Pasquini, S.; Cheadle, E. J.; Carta, L.; Jackson, A. M.; Lemoine, N. R.; Vassaux, G. A Recombinant *E. coli* Vaccine To Promote MHC Class I-Dependent Antigen Presentation: Application to Cancer Immunotherapy. *Gene Ther.* **2002**, *9*, 1455–1463.
53. Plotkin, S. A. Correlates of Vaccine-Induced Immunity. *Clin. Infect. Dis.* **2008**, *47*, 401–409.
54. Dogan, I.; Bertocci, B.; Vilmont, V.; Delbos, F.; Megret, J.; Storck, S.; Reynaud, C. A.; Weill, J. C. Multiple Layers of B Cell Memory with Different Effector Functions. *Nat. Immunol.* **2009**, *10*, 1292–1299.
55. Breitfeld, D.; Ohl, L.; Kremmer, E.; Ellwart, J.; Sallusto, F.; Lipp, M.; Forster, R. Follicular B Helper T Cells Express CXC Chemokine Receptor 5, Localize to B Cell Follicles, and Support Immunoglobulin Production. *J. Exp. Med.* **2000**, *192*, 1545–1551.
56. Rasheed, A. U.; Rahn, H. P.; Sallusto, F.; Lipp, M.; Muller, G. Follicular B Helper T Cell Activity Is Confined to CXCR5 (hi)ICOS(hi) CD4 T Cells and Is Independent of CD57 Expression. *Eur. J. Immunol.* **2006**, *36*, 1892–1903.
57. De Filette, M.; Martens, W.; Roose, K.; Deroo, T.; Vervalle, F.; Bentahir, M.; Vandekerckhove, J.; Fiers, W.; Saelens, X. An Influenza A Vaccine Based on Tetrameric Ectodomain of Matrix Protein 2. *J. Biol. Chem.* **2008**, *283*, 11382–11387.
58. Pinto, L. H.; Lamb, R. A. The M2 Proton Channels of Influenza A and B Viruses. *J. Biol. Chem.* **2006**, *281*, 8997–9000.
59. Schotsaert, M.; De Filette, M.; Fiers, W.; Saelens, X. Universal M2 Ectodomain-Based Influenza A Vaccines: Preclinical and Clinical Developments. *Expert Rev. Vaccines* **2009**, *8*, 499–508.
60. El Bakkouri, K.; Descamps, F.; De Filette, M.; Smet, A.; Festjens, E.; Birkett, A.; Van Rooijen, N.; Verbeek, S.; Fiers, W.; Saelens, X. Universal Vaccine Based on Ectodomain of Matrix Protein 2 of Influenza A: Fc Receptors and Alveolar Macrophages Mediate Protection. *J. Immunol.* **2011**, *186*, 1022–1031.
61. Geurts van Kessel, C. H.; Willart, M. A. M.; van Rijt, L. S.; Muskens, F.; Kool, M.; Baas, C.; Thielemans, K.; Bennett, C.; Clausen, B. E.; Hoogsteden, H. C.; *et al.* Clearance of Influenza Virus from the Lung Depends on Migratory Langerin(+)CD11b(−) but Not Plasmacytoid Dendritic Cells. *J. Exp. Med.* **2008**, *205*, 1621–1634.